## Electronic Supplementary Information

# Solvent-free temperature gradient melt formation of efficient visible-to-UV photon upconversion organic films with subsolar threshold and over 100 h photostability in air

Riku Enomoto[a,b] and Yoichi Murakami[a,b]*

[a] Laboratory for Zero-Carbon Energy, Institute of Innovative Research, Tokyo Institute of Technology, 2-12-1 Ookayama, Meguro-ku, Tokyo 152-8550, Japan.

[b] Department of Mechanical Engineering, Tokyo Institute of Technology, 2-12-1 Ookayama, Meguro-ku, Tokyo 152-8552, Japan.

*Corresponding Author. E-mail: murakami.y.af@m.titech.ac.jp

## List of Contents

## 1. Experimental details

### 1.1 Chemicals

PPO (99%) was purchased from Sigma–Aldrich and used as received. CBDAC (> 98%) was purchased from TCI and the methanol solution ($4\times10^{-4}$ M) was passed through a polytetrafluoroethylene membrane filter (SLLGX13NL, Merck-LG; pore size: 200 nm) to remove any particulate matter that might have been in the supplied CBDAC; this methanol solution was used in the sample preparation.

### 1.2 Preparation of PPO–CBDAC blend

The filtered methanol solution of CBDAC ($4 \times 10^{-4}$ M) was added to PPO powder by using a mechanical pipette to form a mixture of PPO and CBDAC (30,000:1 in mol). This mixture was then evacuated in a vacuum chamber, which was connected to a dry scroll pump (nXDS15i, Edwards, UK; down to 2 Pa), for 15 min to remove the methanol. Finally, the mixture was ground into a fine powder with a quartz mortar to obtain a uniform blend of PPO and CBDAC.

### 1.3 Glass substrate and treatment

Round glass substrates (diameter: 12 mm, thickness: 0.7 mm) were purchased from Matsunami Glass Ind., Ltd., Japan. These substrates were made of alkali-free glass (EAGLE XG, Corning, USA). Prior to use, one surface of the substrate was coated with an aluminum thin film (thickness: 50 nm) that served as a light reflection layer during photophysical measurements. The aluminum deposition was achieved with a vacuum evaporator (VTR-350M/ERH, ULVAC, Japan). However, for the optical microscope observations (Fig. 2a in the main text and Fig. S8) in which a transmission illumination from the bottom was used, we used glass substrates without aluminum deposition. During the formation of the sample organic film ("film" hereafter) using our apparatus (described in Section 1.4), the bare glass surface contacted the PPO–CBDAC blend described in Section 1.2; whereas the aluminum-deposited side contacted the stainless steel (SUS) stage of the apparatus.

### 1.4 Apparatus for film formation and operation procedures

A graphic and photograph of the film formation system originally developed by us for this study are shown in Fig. S1a and S1b, respectively. The main parts were placed inside a vacuum chamber, which mainly comprised a "NW63-flanged, 4-way cross" made of Duran glass. The core portion of the apparatus consists of two SUS stages, heat sinks, and mechanics that continuously applied a compression force to the blend of PPO and CBDAC during the process. Each SUS stage has five thermocouples allocated at an interval of 6 mm and two rod heaters, all of which were embedded in the stage (Fig. S1). The powers of the two rod heaters, one for the higher temperature end and the other for the lower temperature end, were independently controlled with digital temperature controllers (Fig. S1). Stacked copper foils connect were attached to the cold end of the stages and the other ends were fixed to a Peltier cooler maintained at 5 °C (Fig. S1b) such that these copper foils serve as heat sinks, which are necessary for the temperature control. The temperature profile over the stage was monitored and recorded by using those thermocouples and a data logger (Fig. S1b and S2).

The operational procedure was as follows. First, a SUS spacer ring (thickness: 0.2 mm, inner diameter: 8 mm) was placed on the glass substrate (cf. Section 1.3). Then, 32 mg of the PPO and CBDAC powder blend (cf. Section 1.2) was mounted inside the spacer ring and the other glass substrate was placed onto it, which is termed "stack" hereafter. The periphery of the stack was sealed with a perfluoro elastomer O-ring to prevent loss of material during the process carried out under vacuum. This "stack + O-ring" was then sandwiched by the two SUS stages (Fig. S1a). During the process, the chamber was evacuated with a dry scroll pump (nXDS15i, Edwards, UK) and a compression force of ca. 200 N was applied normal to the stack with a mechanical spring (Fig. S1). The purpose of the vacuum was to eliminate influence from the laboratory environment and prevent inclusion of gas bubbles in the fabricated film. The purposes of applying the compression force were to ensure that the (i) O-ring was effective, (ii) obtained film had the same thickness as that of the ring spacer (i.e., 200 μm), and (iii) SUS stage and the substrate were in good thermal contact.

When the stack was taken out of the chamber, the fabricated film was adhered only to one of the substrates because the adhesion force of the film to the substrate was weaker

than the integrity of the film. Therefore, all characterizations—including observations with a microscope—were carried out in the state that one surface of the film was exposed to ambient air. Prior to photophysical measurements (including UC performance evaluations), the film was annealed in dry nitrogen gas at 66 °C for 30 min for the purpose of improving the crystallinity of the sample.

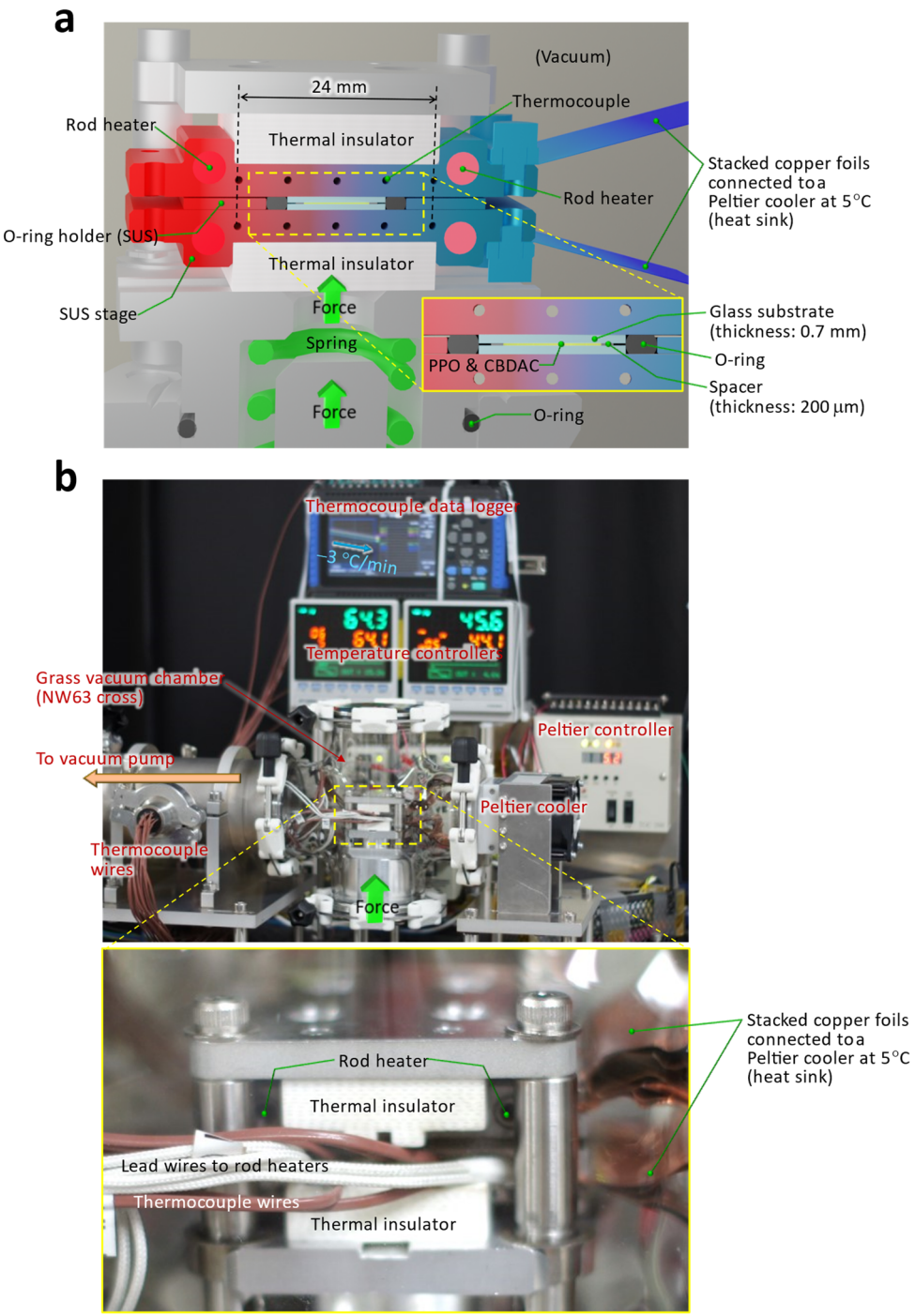


**Fig. S1**. A CAD graphic (a) and photograph (b) of the film fabrication apparatus originally designed and developed by us to carry out this study.

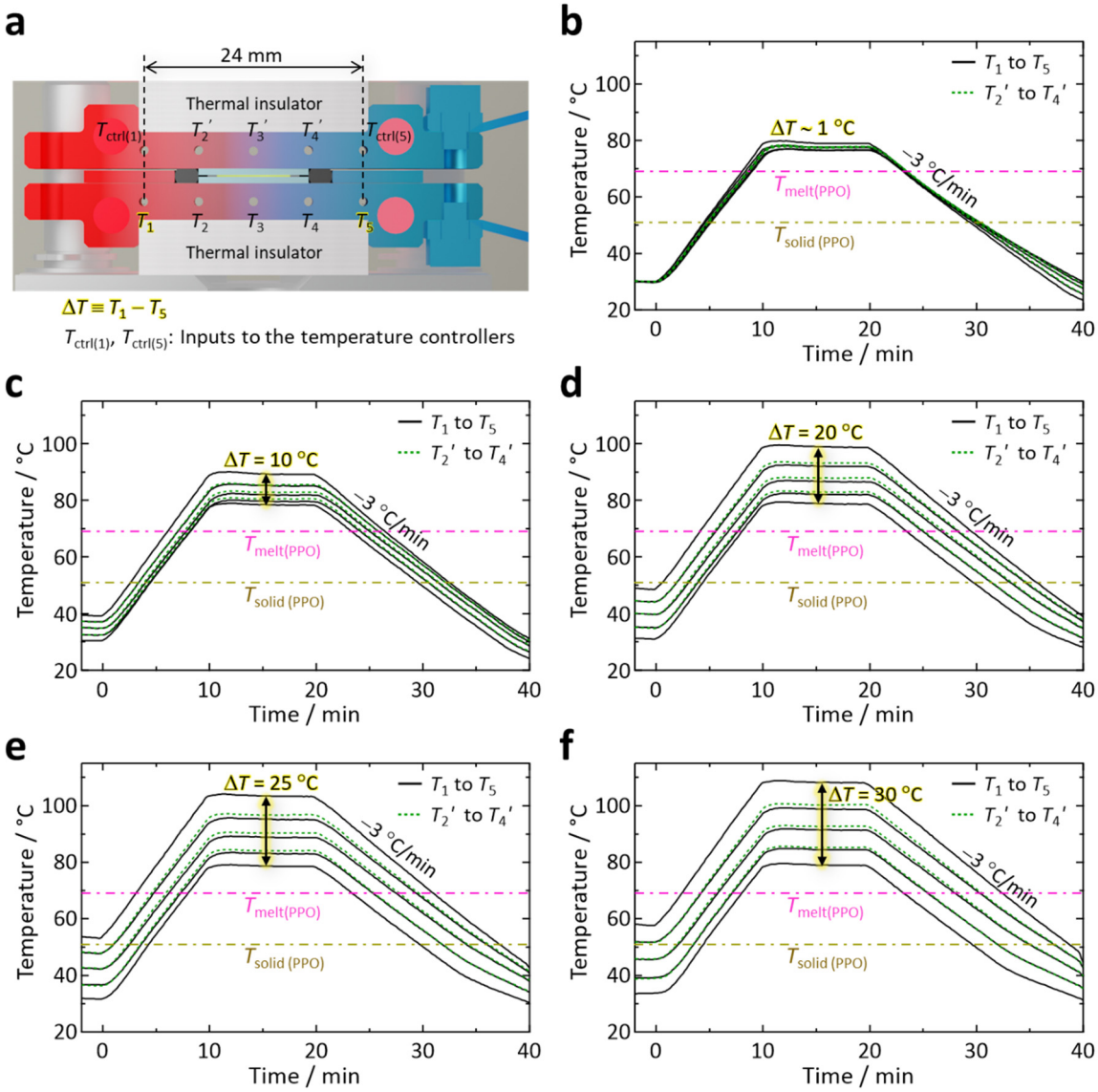


**Fig. S2**. (a) Nomenclature of the thermocouples embedded in the SUS stages and definition of $\Delta T$. (b)–(f) The time dependent temperature profiles recorded with the thermocouples for the cases of $\Delta T$ = "~ 1 °C," 10 °C, 20 °C, 25 °C, and 30 °C, respectively. In these panels, the melting and solidification temperatures of PPO, denoted $T_{melt(PPO)}$ and $T_{solid(PPO)}$, respectively, are indicated.

### 1.5 Optical microscope observations

Optical microscope observations in this study were carried out with a polarizing microscope (BX-53, Olympus, Japan) by transmission illumination. The polarized light microscopy observations in Fig. 2a in the main text were performed with a crossed-Nicols configuration.

### 1.6 Differential scanning calorimetry (DSC)

The melting and solidification temperatures (denoted $T_{melt}$ and $T_{solid}$, respectively) of PPO, CBDAC and the PPO–CBDAC blend (cf. Section 1.2) were evaluated with a differential scanning calorimeter (DSC-60, Shimadzu, Japan) equipped with aluminum seal cells at a temperature scan rate of 5 °C/min. The results are shown in Fig. S6.

### 1.7 Powder X-ray diffraction (PXRD) measurements

PXRD measurements were performed with an X-ray diffractometer (SmartLab, Rigaku, Japan) at 298 K with Cu $K_\alpha$ radiation. The sample was manually cut into a fine powder with a razor blade and then annealed at 66 °C for 30 min in dry nitrogen gas to eliminate the potential influences during the cutting. Then, ca. 50 mg of it was sandwiched between two Mylar thin films, set in the measurement mount. The mount was rotated at 120 rpm during the measurements. The PXRD patterns shown in Fig. 2b in the main text were acquired at a scan step of 0.01° and scan speed of 0.5°/min. The Pawley and Rietveld refinements were carried out with *Reflex module* of Materials Studio 2022 software; the results are presented in Fig. 2c in the main text, Fig. S9, and Table S3.

### 1.8 Photoemission measurements by continuous-wave (CW) laser excitation

The photophysical measurements in Figs. 3a, 3b, and 3d in the main text were carried out with the setup described in Fig. S3, containing a 440-nm CW laser (TECBL-30GC-440, World Star Technologies in Canada). The laser beam diameter and beam profile at the sample position was ca. 3 mm and top-hat shape, respectively. The sample substrate was held at an angle slightly (~5°) deviated from the normal incidence of the laser beam as schematically shown in Fig. S3. The photoemission from the sample was collected and focused onto an entrance slit of a monochromator (SP-2300i, Princeton Instruments, USA) by using two achromatic lenses. The spectrum was recorded with an arrayed CCD detector (PIXIS:100BR, Princeton Instruments) mounted at the exit of the monochromator.

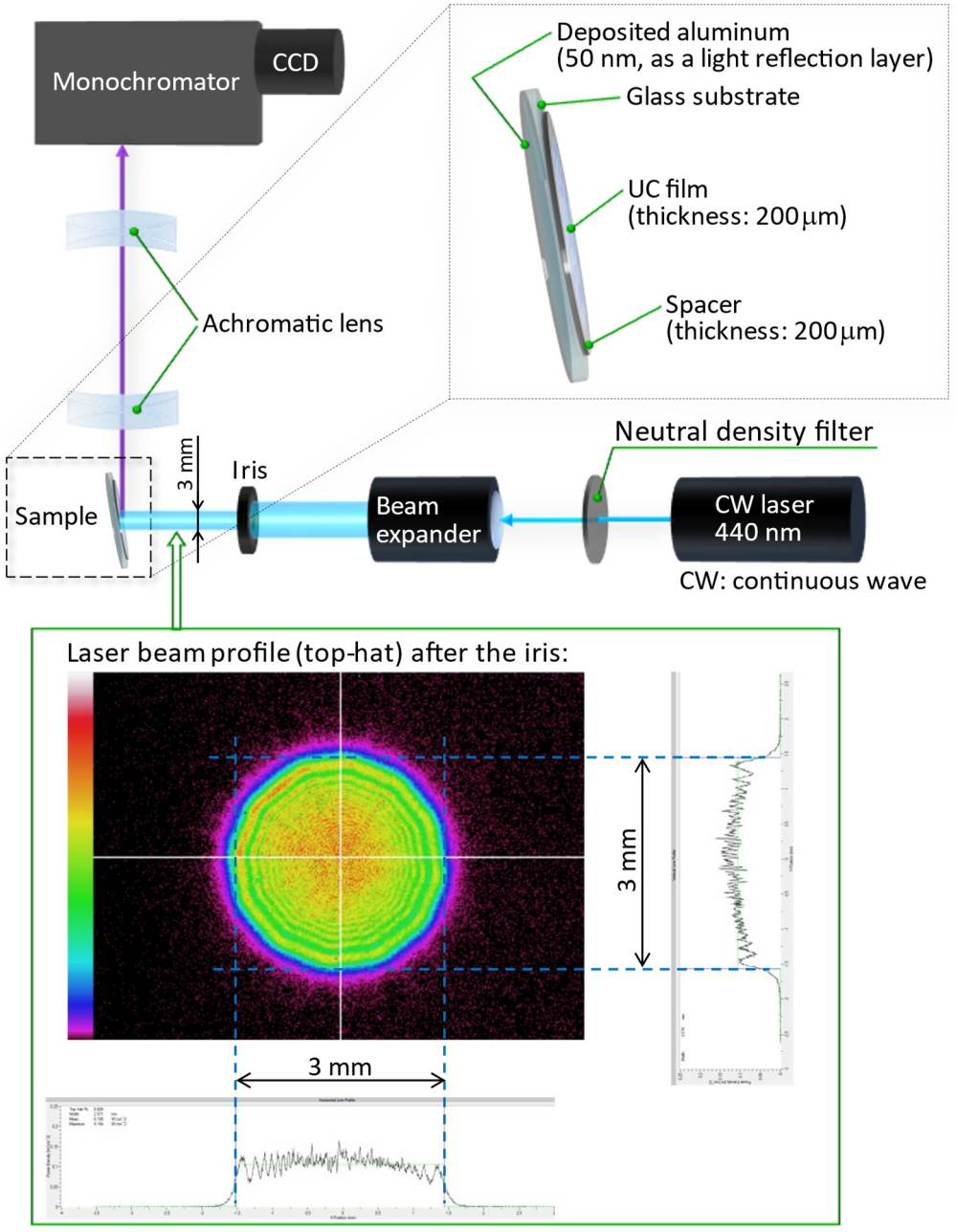


**Fig. S3**. Schematic of the experimental setup for the photoemission measurements with 440-nm CW excitation. The bottom shows the laser beam profile acquired near the sample position.

### 1.9 Excitation spectrum measurements

To acquire the excitation spectrum, the UC film was irradiated with the pulsed light generated from a wavelength-tunable optical parametric oscillator (NT-242, EKSPLA, Lithuania; pulse duration: ca. 3 ns, repetition rate: 100 Hz). The excitation spectra shown in Fig. 3a in the main text were obtained by plotting the UC emission intensity integrated over the range of 380–390 nm against the wavelength of the laser light, which was varied from 410–488 nm maintaining the pulse energy to be 10 μJ.

### 1.10 Determination of $\Phi_{UC}$

First, we determined the quantum yield of fluorescence from CBDAC ($\Phi_{F(S)}$ in Scheme 1 in the main text) in the polycrystalline film of PPO formed on the round grass substrate under the $\Delta T$ = 20 °C condition (hereafter, UC sample). This UC film consisted of CBDAC and PPO in the mole ratio of 1:30,000 (*cf.* Section 1.2). To determine $\Phi_{F(S)}$, an absolute photoluminescence quantum yield spectrometer equipped with an integration sphere (Quantaurus-QY, Hamamatsu, Japan) was used with the excitation wavelength of 440 nm (*i.e.*, the same wavelength as that used for the UC emission measurements). First, the baseline was acquired placing a reference sample, which was a polycrystalline film of PPO formed on the substrate under the $\Delta T$ = 20 °C condition without containing CBDAC, in the integration sphere. Then, the measurement was carried out placing a UC sample in the integration sphere. From the measurements of five UC samples prepared with $\Delta T$ = 20 °C, we have determined $\Phi_{F(S)}$ to be 5.1±0.23%; 5.1% is the average and 0.23% is the standard deviation calculated from the five values. This value (5.1±0.23%) has not been corrected by the self-absorption by CBDAC. Notably, therefore, *this $\Phi_{F(S)}$ value is lower than the true value*, *because the use of an integration sphere unavoidably accompanies multiple self-absorptions of the fluorescence by the chromophore*, as revealed by the overlap between the fluorescence spectrum and excitation spectrum of CBDAC indicated in Fig. S10.

During an irradiation of a sample with a laser light of $\lambda$ = 440 nm exhibiting a top-hat beam profile (*cf.* Fig. S3), the spectra of a UC fluorescence from PPO and a prompt fluorescence from CBDAC were simultaneously acquired as indicated by Fig. 3a in the main text. All emission spectra in this report have been corrected by the wavelength-

dependences of diffraction efficiency of a grating in the monochromator and the quantum efficiency of an arrayed CCD detector (PIXIS:100BR, Princeton Instruments). We denote thereby corrected fluorescence spectrum by $I(\lambda)$.

Hereafter, we use the subscripts "UC" and "F(S)" to represent UC fluorescence from PPO and prompt fluorescence from CBDAC, respectively. During measurements using the setup illustrated by Fig. S3, *both types of fluorescence were simultaneously emitted from an identical irradiation spot on the same sample resulted from an identical photoexcitation of CBDAC* by a laser at 440 nm (*cf.* Section 1.8); this situation is much simpler than the typical situation of a conventional referencing method in which light-absorbing chromophores, excitation wavelengths, absorbances at the excitation wavelength, and solvents (or refractive indexes) are generally different between a "sample" and a "reference."

According to the IUPAC dentition, a quantum yield ($\Phi$) is defined by[S1]

$$\Phi = \frac{\#\text{ of events}}{\#\text{ of absorbed photons}} . \tag{S1}$$

In the present study, the "events" is emission of UC photons and hence

$$\Phi_{\mathrm{UC}} = \frac{\#\text{ of emitted UC photons } (\equiv\ N_{\mathrm{UC}})}{\#\text{ of absorbed photons}} , \tag{S2}$$

which means that the maximum of $\Phi_{\mathrm{UC}}$ is 50% by definition. Similarly,

$$\Phi_{\mathrm{F(S)}} = \frac{\#\text{ of emitted fluoresence photons from CBDAC } (\equiv\ N_{\mathrm{F(S)}})}{\#\text{ of absorbed photons}} . \tag{S3}$$

During the measurement for determining $\Phi_{\mathrm{UC}}$, the denominators of eqns (S2) and (S3) have a common value because a UC fluorescence from PPO and a prompt fluorescence from CBDAC were simultaneously acquired as a result of an identical photoexcitation as mentioned above. Therefore, by combining eqns (S2) and (S3), we obtain

$$\Phi_{\mathrm{UC}} = \Phi_{\mathrm{F(S)}} \frac{N_{\mathrm{UC}}}{N_{\mathrm{F(S)}}} . \tag{S4}$$

Note that no reabsorption of UC photons by the material has been corrected in our calculation of $\Phi_{\mathrm{UC}}$ via eqn (S4).

As explained in the main text, we have defined photoemission in the range of $\lambda \leq$ 425 nm as UC emission; no UC emission was observed for the wavelength shorter than

350 nm. The fluorescence from CBDAC was ranged in 450 nm ≤ $\lambda$ ≤ 700 nm. Therefore, because a CCD accumulates photon-induced charges,

$$\frac{N_{\mathrm{UC}}}{N_{\mathrm{F(S)}}} = \frac{\int_{350}^{425} I(\lambda)d\lambda}{\int_{450}^{700} I(\lambda)d\lambda} \ . \tag{S5}$$

By substituting eqn (S5) into eqn (S4), we obtained $\Phi_{\mathrm{UC}}$. As mentioned above, $\Phi_{\mathrm{F(S)}}$ had been determined to be 5.1±0.23%. Therefore, at least (0.23/5.1)×100 = 0.045 ≅ 5% uncertainty should have accompanied the $\Phi_{\mathrm{UC}}$ reported here. Notably, the ratio $N_{\mathrm{UC}}/N_{\mathrm{F(S)}}$ is independent of the incident light polarization (*cf.* Section 10) and thus unaffected by the anisotropic crystal growth in the present UC samples.

In this scheme, we have assumed that the wavelength dependence of refractive index ($n$) of the PPO film is small or negligible, whereas this factor might affect photoemission quantum yield.[S2,S3] We have found no literature that reported the wavelength dependence of $n$ of solid PPO. However, we consider that this effect should be negligibly small because polycrystalline nature of the present samples (*cf.* Fig. 2a in the main text) causes diffusive photoemission out of the film. In fact, we have confirmed using an optical fiber as a light collector that the intensity distribution of photoemission from the sample was hemispherically isotropic. Such a situation essentially differs from an ideal situation where ray-traces of emitted fluorescence obey Snell's law over a flat and large air–solid interface, which was assumed in refs. S2 and S3.

Notably, when we measured the powder of 9,10-diphenylanthracene (DPA; supplied from TCI, sublimation grade, purity > 99%) using the same absolute photoluminescence quantum yield spectrometer (Quantaurus-QY, Hamamatsu), $\Phi_{\mathrm{F(S)}}$ was measured to be 81%, which is lower than previously reported $\Phi_{\mathrm{F(S)}}$ values for DPA powders (85%) and DPA crystals (95%).[S4] In addition, as mentioned above, because $\Phi_{\mathrm{F(S)}}$ was determined using an integration sphere and the value has not been corrected by the effect of self-absorption, this value ($\Phi_{\mathrm{F(S)}}$ = 5.1±0.23%) is considered to be lower than its true value. These facts suggest that, especially because of our use of eqn (S4) for the latter, the values of $\Phi_{\mathrm{UC}}$ presented in this report have been underestimated.

Finally, we have additionally measured $\Phi_{\mathrm{F(S)}}$ values of four different samples prepared with the condition of $\Delta T$ ~ 1 °C. The results were $\Phi_{\mathrm{F(S)}}$ = 5.2±0.19% (0.19%:

standard deviation), which agreed well with the values obtained for the $\Delta T$ = 20 °C condition.

### 1.11 Photoemission measurements with a solar simulator system

Simulated air mass 1.5 (AM1.5) sunlight was generated with a solar simulator (HAL-320, Asahi Spectra, Japan). As shown in Fig. S4, the sample was placed on a glass slide, mounted on a three-axis translation stage, and irradiated with a simulated sunlight that had passed through a long-pass filter (BLP01-405R-25, Semrock, USA) placed on a square aperture (ca. 1.5 cm × 1.5 cm) in the absorption plate. Through this aperture, only the central uniform portion of the simulated sunlight was extracted. This long-pass filter transmits only the spectral range of $\lambda > 413$ nm as shown by the optical density (O. D.) and transmission spectra in Fig. S5. The detailed procedure and conditions were the same as those used in our previous report.[S5]

The intensity of the simulated sunlight at the sample position was carefully set as follows. First, without the long-pass filter, a one-sun checker (CS-20, Asahi Spectra) was placed at the sample position and the intensity there was set to "one-sun" intensity by adjusting the output power of the solar simulator. Then, the long-pass filter was placed on the aforementioned aperture. Subsequently, because this long-pass filter exhibited ca. 98% transmittance over the wavelength range of the optical absorption by CBDAC (Fig. S5 and Fig. 3a in the main text), the output power of the solar simulator was increased by 1.02× to compensate for the reduction of the light intensity at the sample position caused by insertion of this long-pass filter. This state was defined as 1⊙ (one-sun) intensity at the sample position. All of the data were acquired in the dark to avoid any potential artifacts that could arise from environmental light.

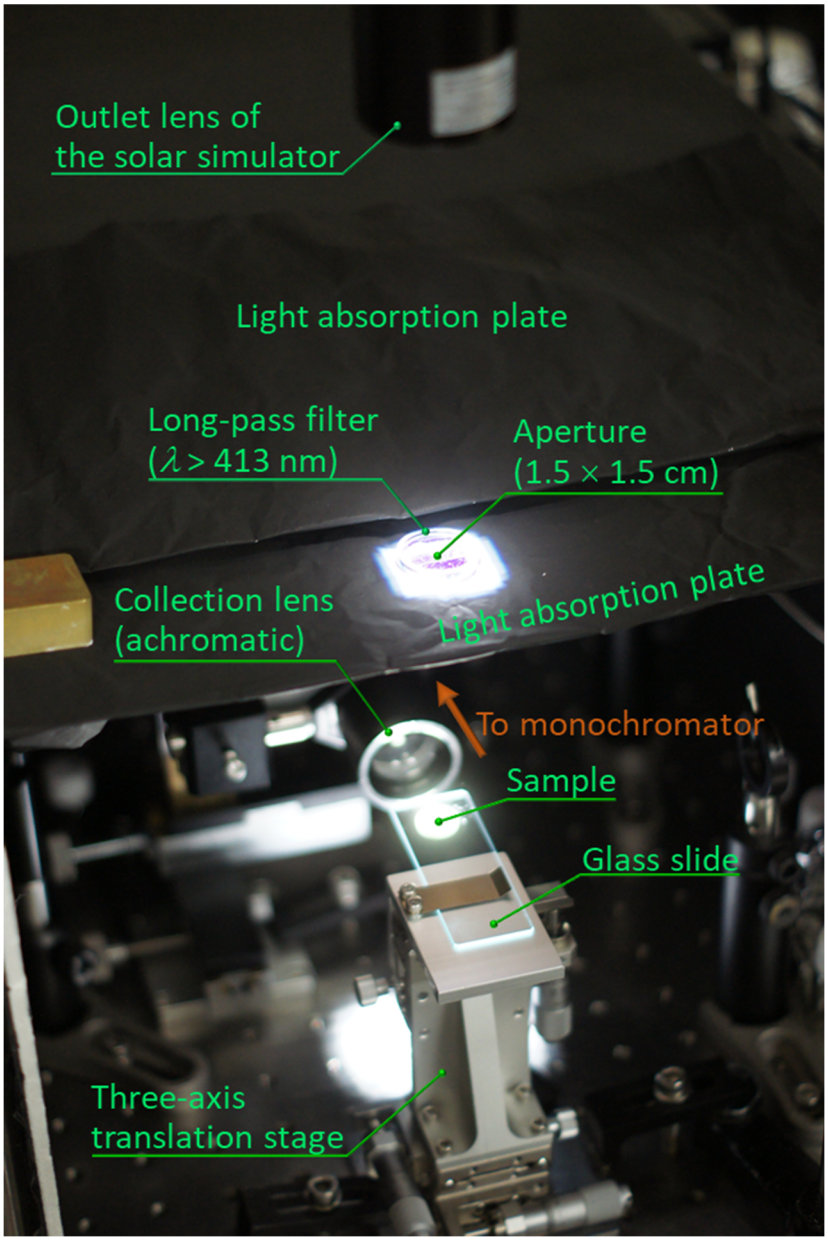


**Fig. S4**. Photograph of the experimental setup for the photoemission measurements with simulated sunlight generated with the solar simulator.

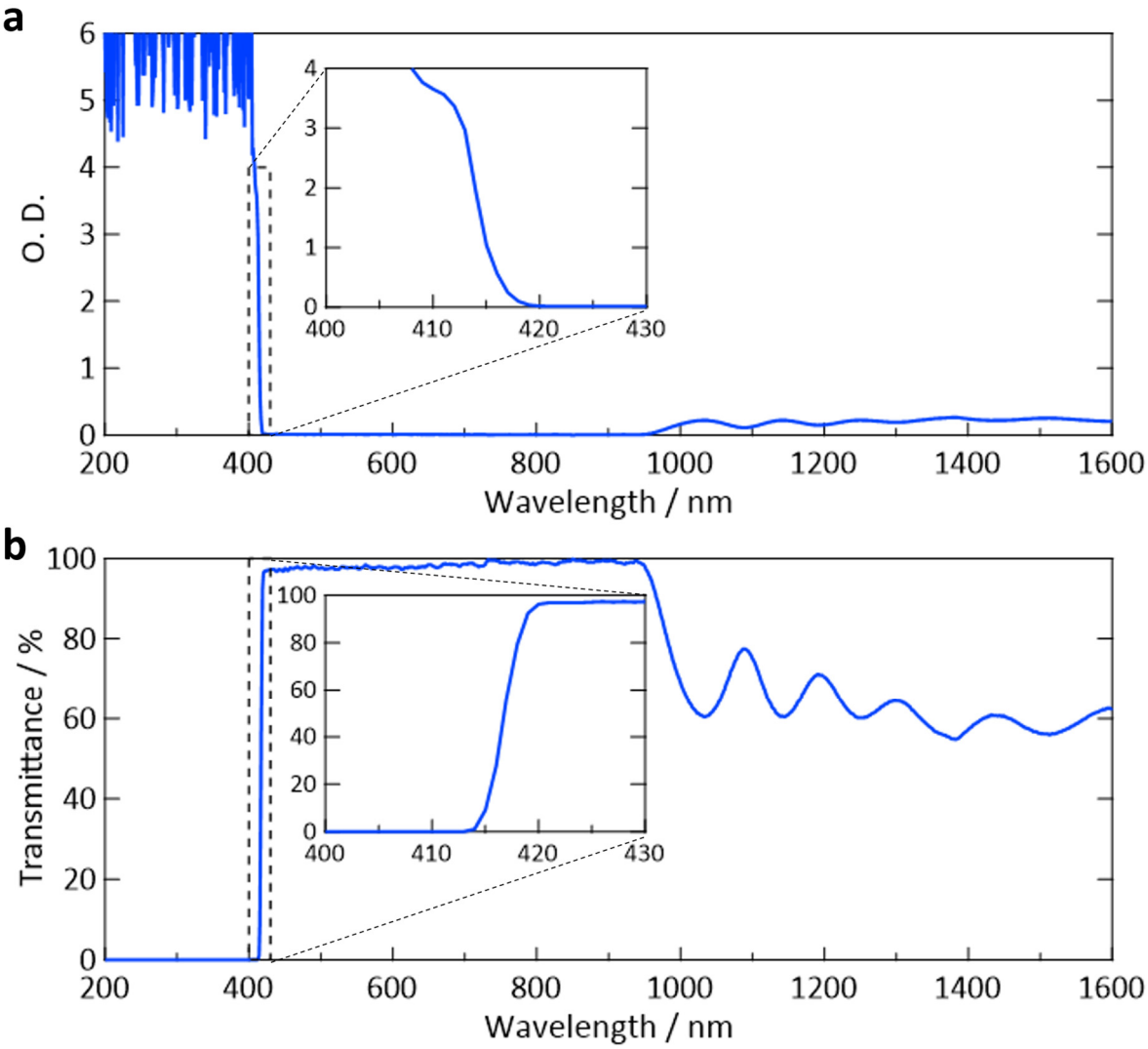


**Fig. S5**. (a) Optical density and (b) transmittance spectra of the long-pass filter used in combination with the solar simulator in Fig. S4.

### 1.12 Transient photoemission measurements by pulsed laser excitation

For transient photoemission measurements carried out for Figs. S11 and S12, 463-nm light pulses (pulse duration: ca. 3 ns, repetition rate: 40 Hz) generated from the aforementioned optical parametric oscillator were used. The UC emission from the sample was collected and introduced into the monochromator by using the same optical collection path as that shown in Fig. S3. However, in this case, the time-dependent emission intensity change was recorded with a photomultiplier tube (H11461, Hamamatsu, Japan) mounted at the exit of the monochromator.

## 2. Other combinations of sensitizer–annihilator tested

**Table S1.** Some examples of combinations of sensitizer and annihilator tested.

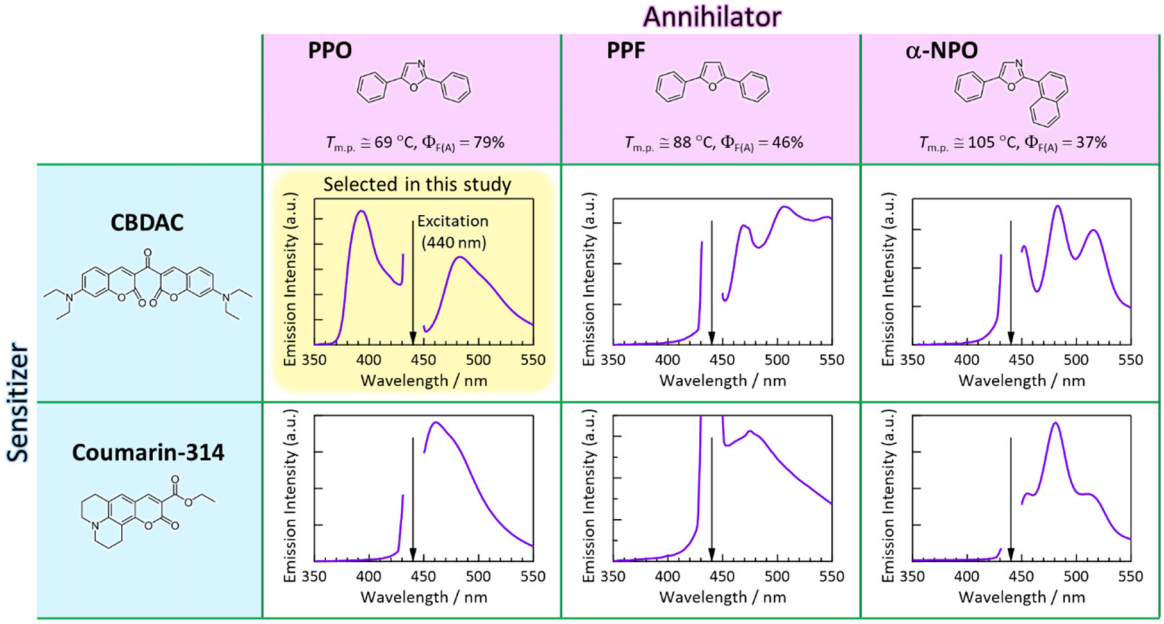


## 3. Phase change behaviors of PPO and CBDAC

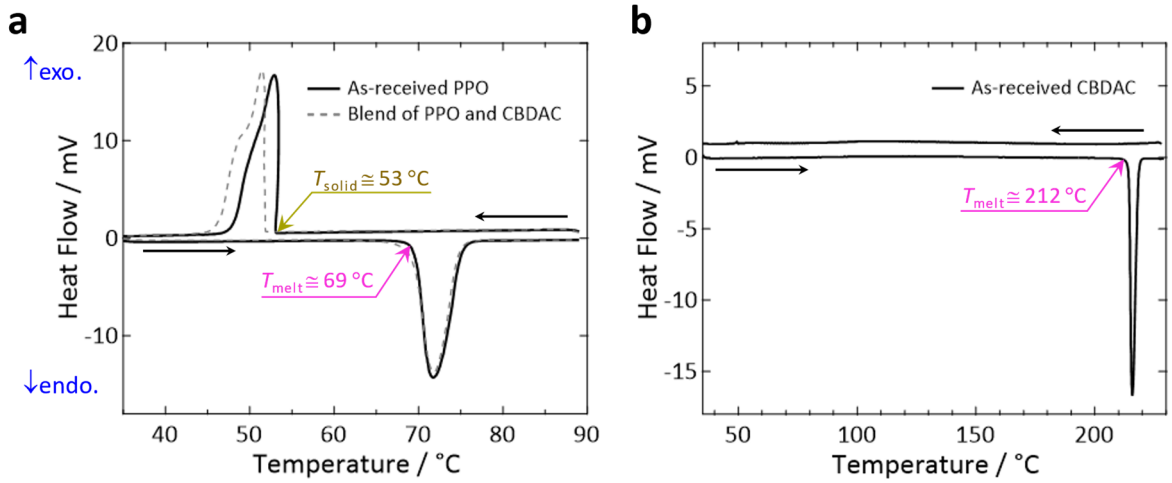


**Fig. S6**. DSC signals acquired for (a) as-received PPO (solid curves) and the 30,000:1 (mol) blend of PPO and CBDAC (dashed curves) and (b) as-received CBDAC. For each case, approximately 8 mg of sample was sealed in an aluminum cell. The measurements were carried out at a scan rate of 5 °C/min flowing 35 sccm of dry nitrogen gas. No solidification peak was found for CBDAC, presumably because of supercooling.

## 4. Determination of the optimal ratio of CBDAC:PPO

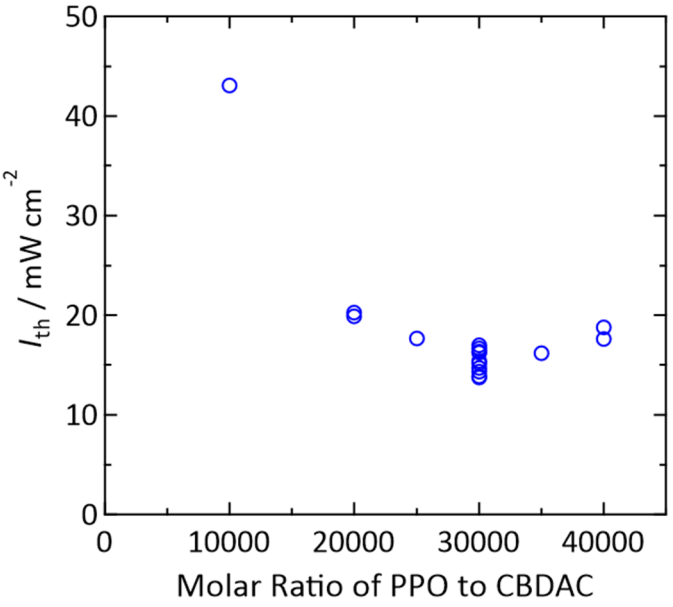


**Fig. S7**. Dependence of the excitation threshold intensity ($I_{th}$) on the mole ratio of PPO to CBDAC. Higher $I_{th}$ for the cases of lower mole ratio might be attributable to the quenching mechanism discussed in ref. S6.

## 5. Results for –1 °C/min and $\Delta T$ = 20 °C

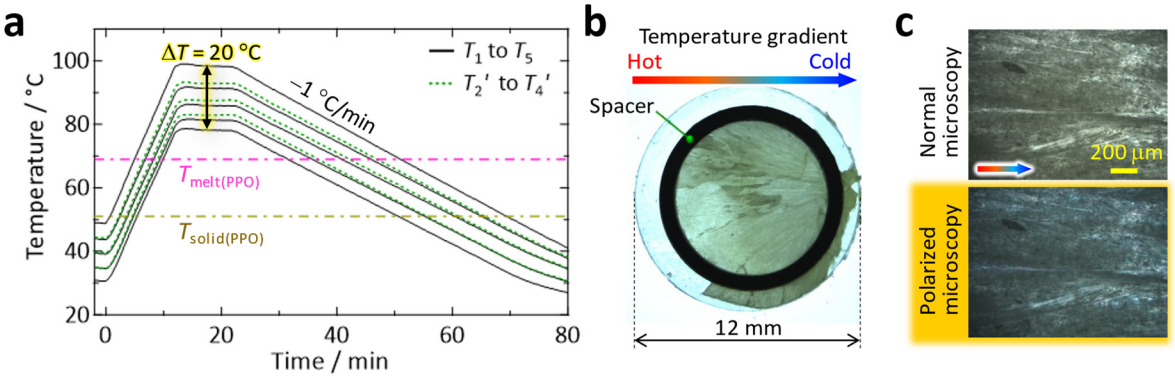


**Fig. S8**. The results for –1 °C/min and $\Delta T$ = 20 °C. (a) The recorded change of the temperature profile applied to the sample. (b) The stereo microscope image of the UC film and (c) the magnified microscope images acquired by transmitted illumination.

## 6. Crystallographic analyses and results

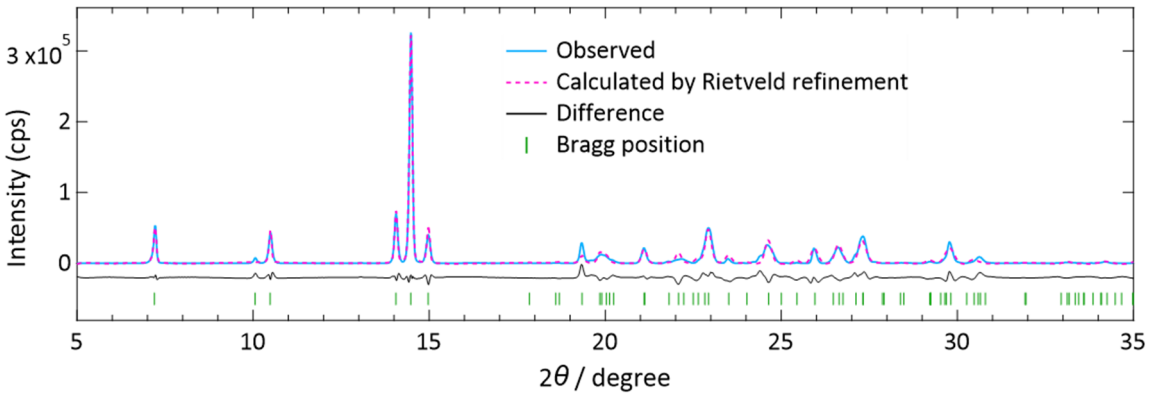


**Fig. S9**. PXRD patterns for the sample fabricated with $\Delta T$ = 20 °C (blue solid line) and the calculated pattern for the structural model after Pawley and Rietveld refinements (pink dashed line). The structure after the refinements and the crystallographic parameters are given in Fig. 2c in the main text and Table S3, respectively.

We performed Pawley and Rietveld refinements on the observed diffraction pattern in Fig. S9 by using the *Reflex module* of the Materials Studio 2022 software. The conditions for the refinements and the results are summarised in Table S2 and Tables S3–S5, respectively.

**Table S2.** Conditions used for the refinements.

| | |
|---|---|
| **2$\theta$ range (°)** | 5–35 |
| **Step size (°)** | 0.01 |
| **Type** | X-ray |
| **Source** | Copper |
| **$\lambda$ (Å)** | 1.540562 |
| **Monochromator** | None |
| **Anom. Dispersion** | No |
| **Polarization** | 0.500 |
| **Refined Motion Groups** | 1 |
| **Refined Distances** | 0 |
| **Refined Angles** | 0 |
| **Refined Torsions** | 2 |
| **Number of Refined DOF** | 8 |

**Table S3.** Crystallographic parameters after the Pawley and Rietveld refinements.

| | **UC film (PPO:CBDAC = 30,000:1, $\Delta T$ = 20 °C)** |
|---|---|
| **Empirical formula** | $C_{15}H_{11}NO$ |
| **Formula weight** | 221.26 |
| **Temperature (K)** | 298 |
| **Crystal system** | Monoclinic |
| **Space group** | $P2_1/c$ |
| ***Z*** | 4 |
| ***a*, *b*, *c* (Å)** | 12.7663, 5.1639, 18.3281 |
| **$\alpha$, $\beta$, $\gamma$ (°)** | 90, 107.3783, 90 |
| ***V* (Å$^3$)** | 1153.11 |
| **$R_{wp}$ (%)** | 12.09 |

**Table S4.** R-factors and total energy output from Reflex Powder Refinement tools.

| | |
|---|---|
| **Final $R_{wp}$ (%)** | 12.09 |
| **Final $R_{wp}$ (without background) (%)** | 12.02 |
| **Final $R_p$ (%)** | 27.98 |
| **Final CMACS (%)** | 8.05 |
| **Forcefield** | Compass III |
| **$R_{wp}$ Weight (%)** | 50.00 |
| **Energy Weight (%)** | 50.00 |
| **Final $R_{comb}$ (%)** | 6.44 |
| **Final *RE* (%)** | 0.80 |
| **Final *E* (kcal/mol)** | 1074.89 |
| **$E$-$E_{min}$ (kcal/mol)** | 3.20 |

**Table S5.** Atomic positions after the Pawley and Rietveld refinements.

| | Atomic coordinates | | | Fractional coordinates | | | |
|---|---|---|---|---|---|---|---|
| | ***x*** | ***y*** | ***z*** | ***u*** | ***v*** | ***w*** | **Refined?** |
| **C1** | 0.3271 | 0.80424 | –0.6775 | 0.3271 | 0.80424 | 0.32251 | Yes |
| **C2** | 0.4298 | 1.04177 | –0.58872 | 0.4298 | 1.04178 | 0.41128 | Yes |
| **C3** | 0.32548 | 1.11843 | –0.59817 | 0.32548 | 1.11844 | 0.40183 | Yes |
| **C4** | 0.27185 | 1.31042 | –0.56368 | 0.27185 | 1.31043 | 0.43632 | Yes |
| **C5** | 0.33353 | 1.46943 | –0.50484 | 0.33353 | 1.46943 | 0.49517 | Yes |
| **C6** | 0.28143 | 1.65491 | –0.47332 | 0.28143 | 1.65491 | 0.52668 | Yes |
| **C7** | 0.16883 | 1.68515 | –0.49943 | 0.16883 | 1.68516 | 0.50057 | Yes |
| **C8** | 0.10664 | 1.52542 | –0.55792 | 0.10664 | 1.52544 | 0.44208 | Yes |
| **C9** | 0.15761 | 1.3402 | –0.59002 | 0.15761 | 1.34022 | 0.40998 | Yes |
| **C10** | 0.27833 | 0.62271 | –0.73915 | 0.27833 | 0.62272 | 0.26086 | Yes |
| **C11** | 0.3463 | 0.45161 | –0.76323 | 0.3463 | 0.45162 | 0.23677 | Yes |
| **C12** | 0.30122 | 0.27065 | –0.81953 | 0.30122 | 0.27067 | 0.18046 | Yes |
| **C13** | 0.18898 | 0.25938 | –0.85307 | 0.18898 | 0.25939 | 0.14693 | Yes |
| **C14** | 0.12117 | 0.43091 | –0.83015 | 0.12117 | 0.43091 | 0.16986 | Yes |
| **C15** | 0.16518 | 0.61335 | –0.77377 | 0.16518 | 0.61335 | 0.22623 | Yes |
| **H16** | 0.49756 | 1.11038 | –0.55406 | 0.49756 | 1.11039 | 0.44594 | Yes |
| **H17** | 0.4121 | 1.4466 | –0.48789 | 0.4121 | 1.44659 | 0.51211 | Yes |
| **H18** | 0.32581 | 1.7667 | –0.43374 | 0.32581 | 1.76669 | 0.56626 | Yes |
| **H19** | 0.13063 | 1.81699 | –0.47918 | 0.13063 | 1.81699 | 0.52082 | Yes |
| **H20** | 0.02693 | 1.54428 | –0.57665 | 0.02694 | 1.54431 | 0.42335 | Yes |
| **H21** | 0.11578 | 1.23099 | –0.63152 | 0.11578 | 1.23101 | 0.36848 | Yes |
| **H22** | 0.42519 | 0.45447 | –0.73896 | 0.42519 | 0.4545 | 0.26103 | Yes |
| **H23** | 0.34777 | 0.1445 | –0.8341 | 0.34777 | 0.14452 | 0.16589 | Yes |
| **H24** | 0.15346 | 0.12509 | –0.88857 | 0.15346 | 0.1251 | 0.11143 | Yes |
| **H25** | 0.04292 | 0.415 | –0.85378 | 0.04291 | 0.41499 | 0.14623 | Yes |
| **H26** | 0.11604 | 0.72315 | –0.75609 | 0.11604 | 0.72314 | 0.24392 | Yes |
| **N27** | 0.43007 | 0.8415 | –0.63945 | 0.43007 | 0.84151 | 0.36055 | Yes |
| **O28** | 0.2588 | 0.96555 | –0.65551 | 0.2588 | 0.96556 | 0.34449 | Yes |

Note: Occupancies of all the atoms were set to 1 during the refinements.

## 7. Absorption and emission spectra in solutions and in solid states

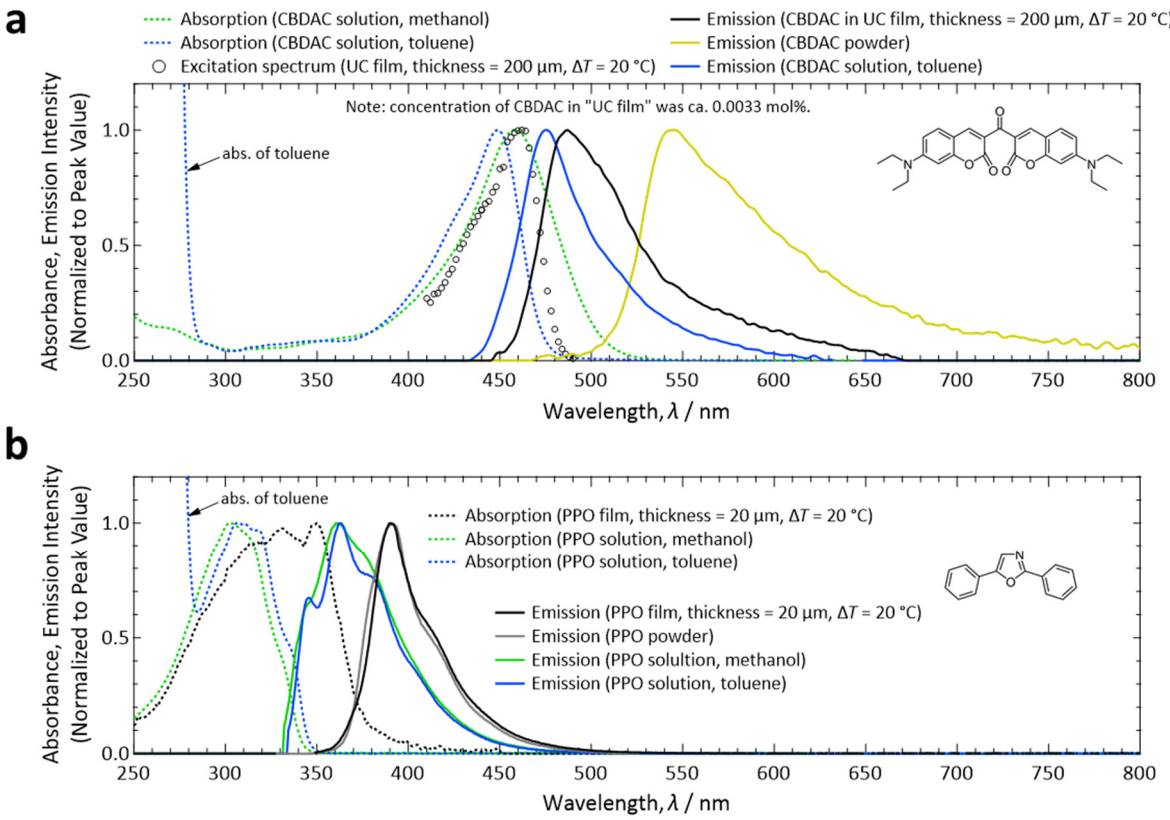


**Fig. S10**. Optical absorption and emission spectra of (a) CBDAC and (b) PPO normalized to the peak value. Absorption spectra of the solutions were acquired using a UV–visible–near-infrared spectrophotometer (UV-3600, Shimadzu) with a quartz cuvette with optical path length of 1 mm. Spectra of fluorescence emission were acquired using an absolute photoluminescence quantum yield spectrometer (Quantaurus-QY, Hamamatsu); no emission was observed from a methanol solution of CBDAC. Concentrations of the solutions: $2 \times 10^{-4}$ M (CBDAC, absorption); $4 \times 10^{-7}$ M (CBDAC, emission); $5 \times 10^{-4}$ M (PPO, absorption); $1 \times 10^{-6}$ M (PPO, emission). In panel (a), "UC film" is a polycrystalline film of PPO doped with CBDAC at the concentration of 0.0033 mol%. The excitation spectrum of CBDAC in the UC film presented in Fig. 3a of the main text (circles) is also shown. In panel (b), "PPO film" is a polycrystalline film of PPO (thickness: 20 μm) without containing CBDAC. In the absorption spectrum of the PPO film, the light-scattering baseline and absorption by the glass substrate, where the latter started to rise from ca. 350 nm, have been subtracted. Note the relatively large redshifts in the fluorescence spectra of the solid-state PPO from the cases of the organic solvent solutions.

## 8. Transient UC emission measurements

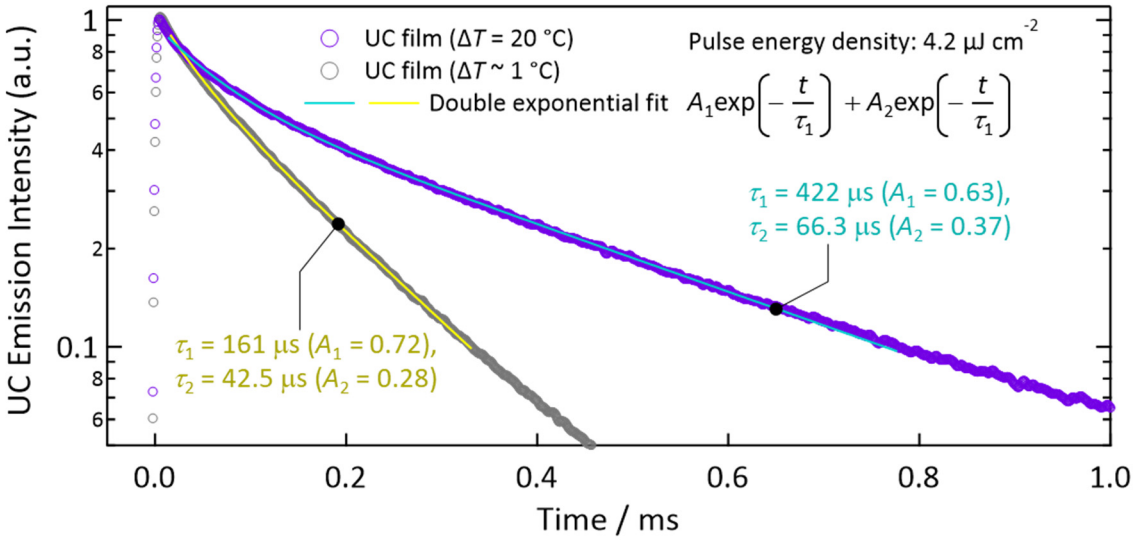


**Fig. S11**. Transient decay curves of the UC emission intensities from the samples and the curve fits with a double-exponential function. See Section 1.12 for experimental details. The excitation pulse energy density was 4.2 μJ $cm^{-2}$.

In Fig. S11, we obtained nonlinear decay curves, which were fitted well by double-exponential decay functions. Because the pulse energy density (4.2 μJ $cm^{-2}$) used there was rather low from our previous experience of investigating the excitation pulse energy dependence of transient UC emission decays in liquid samples,[S7] these nonlinear decays were not considered to arise from the intense pulse excitation studied previously.[S7] To confirm this point, we conducted additional experiments with further lowered excitation pulse energy density of 1.4 μJ $cm^{-2}$. The results (Fig. S12) indicate that the decay curves were the same as those obtained with 4.2 μJ $cm^{-2}$, indicating that the nonlinear decays in Fig. S11 cannot be attributed to an intense excitation.

Although we do not have definite explanations for the origins of the fast and slow decays at present, we provisionally attribute the fast decay component to a first-order depopulation of triplet excitons within a crystalline domain and the slow decay component to the depopulation of the excitons on grain boundaries of the polycrystalline UC film.

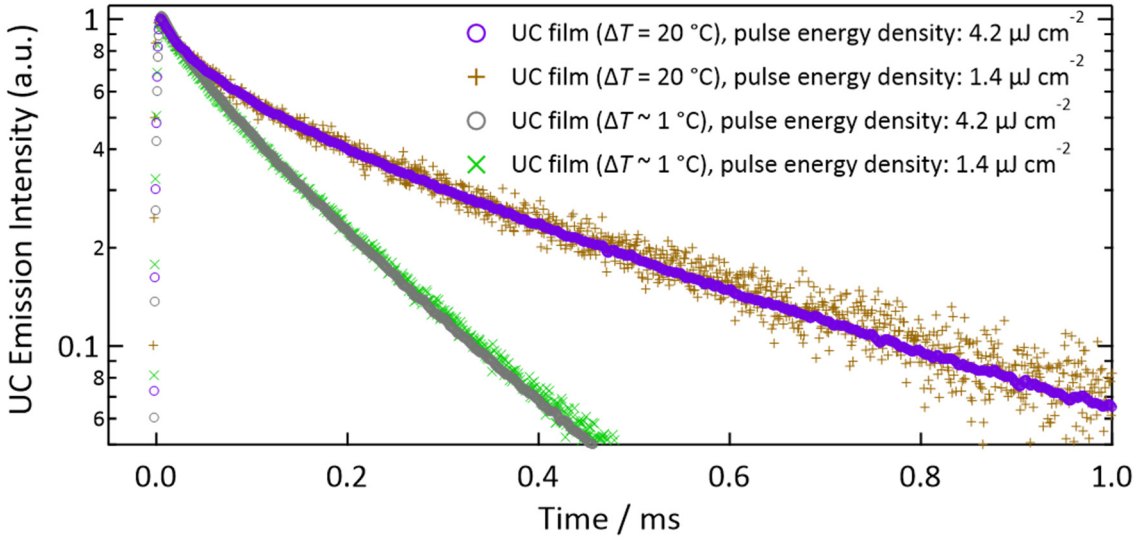


**Fig. S12**. Comparison of the transient decay curves of the UC emission intensities acquired at the pulse energy density of 4.2 and 1.4 μJ cm$^{-2}$, presented for interpreting the results of Fig. S11.

## 9. Distribution of UC and CBDAC fluorescence emissions along temperature-gradient direction

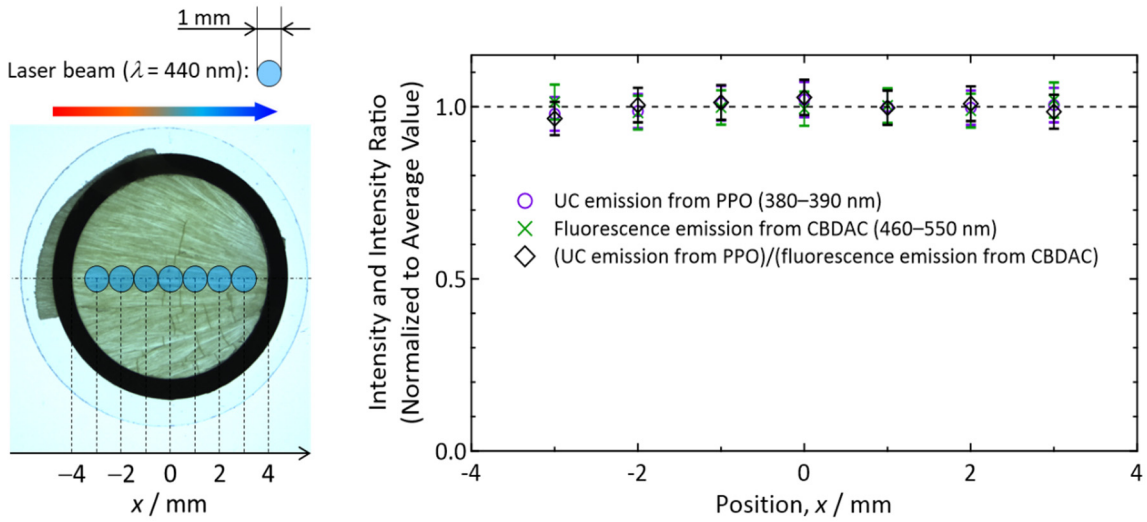


**Fig. S13**. Spatial distribution of the emission intensities along the direction of applied temperature gradient (*x*-direction) on the UC film prepared with $\Delta T$ = 20 °C. The measurement was carried out using a laser spot of 1 mm in diameter ($\lambda$ = 440 nm, intensity: 70 mW cm$^{-2}$) as shown on the left. In the graph, the vertical-axis values have been normalized to the average value. The results indicate independence of the emission intensities along the *x*-position.

## 10. Influence of anisotropic crystal growth on emissions

Because crystals consisting the UC films were directionally grown (*cf*. Fig. 2a) and the excitation laser light ($\lambda$ = 440 nm, *cf*. Section 1.8) was linearly polarized, we carried out the following two types of experiments to elucidate the influence of the anisotropy.

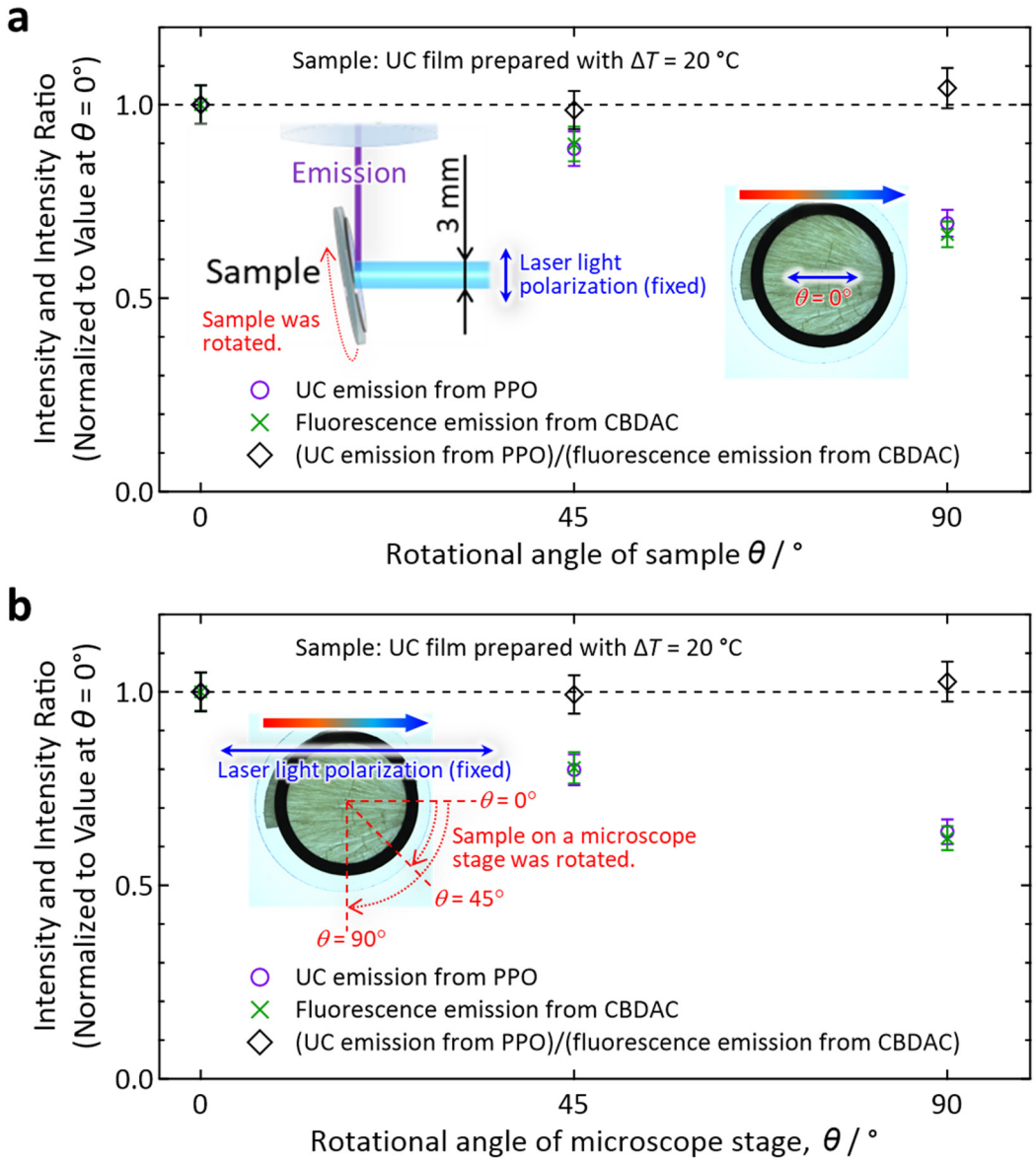


**Fig. S14**. Dependence of UC emission and CBDAC fluorescence intensities on incident light polarization investigated for a UC sample prepared with "$\Delta T$ = 20 °C" condition using a linearly polarized laser light at $\lambda$ = 440 nm. (a) Results of experiment with the sample mounted in the measurement setup of Fig. S3. (b) Results of experiment with the sample placed on a rotational stage of a polarizing microscope (BX-53, Olympus) under a 10× objective lens. In both types of experiments, $\theta$ = 0° was defined for the situation in which the direction of the crystal growth (*i.e.*, direction of the temperature gradient applied) matched the direction of the polarization of the laser light as illustrated in the insets of these panels.

In the first type of experiment, we mounted the "$\Delta T$ = 20°C" sample on the sample holder of the setup illustrated by Fig. S3 and measured emission intensities by changing the rotational angle ($\theta$) of the sample in the holder. In this experiment, $\theta$ = 0° corresponds to our standard means of mounting a sample in which the direction of the crystal growth (*i.e.*, direction of the temperature gradient applied) matched the direction of the linear polarization of the excitation laser light. The emission from the sample was collected by an achromatic lens as illustrated in Fig. S3. Notably, *the emission from the sample was completely depolarized* because we have checked it by setting a Glan-Taylor polarizer between the two achromatic lenses in the emission path (see Fig. S3). The experimental configuration is depicted in the inset of Fig. S14a. We compared the emission intensities of the UC fluorescence from PPO and the prompt fluorescence from CBDAC at $\theta$ = 0°, 45°, and 90°. As indicated by Fig. S14a, both emission intensities were maximal when the direction of the incident light polarization matched the direction of the crystal growth (*i.e.*, when $\theta$ = 0°). As $\theta$ was increased to 90°, the emissions were weakened. Notably, these emission intensities varied similarly with $\theta$ and their ratio was independent of $\theta$.

In the second type of the experiment, we placed a sample prepared with "$\Delta T$ = 20 °C" on the rotational stage of a polarizing microscope (BX-53, Olympus). Using a 10× objective lens, a CW laser light ($\lambda$ = 440 nm) with a top-hat beam profile was focused onto the sample with spot diameter of 50 μm. The incident laser light was linearly polarized on the sample; the direction of the polarization there was identified using a polarizer. As depicted in the inset of Fig. S14b, $\theta$ = 0° was defined for the situation in which the direction of the crystal growth coincided with the direction of the polarization of the incident laser light on the sample. As indicated by Fig. S14b, also at this time, $\theta$ = 0° resulted in maximal emissions for both the UC emission from PPO and the fluorescence from CBDAC. The ratio between these emission intensities was independent of $\theta$.

These results have brought us two findings. (i) UC emission was maximal when the direction of the crystal growth and the direction of the laser light polarization were matched. (ii) The ratio of intensities of the UC fluorescence from PPO to the fluoresce from CBDAC was independent of $\theta$. Point (ii) is an especially important point when $\Phi_{UC}$ is determined by the method described in Section 1.10.

## 11. Derivation of the excitation rate corresponding to $I_{th}$

Absorbance $A$ is expressed by

$$A = \varepsilon C l \tag{S6}$$

where $\varepsilon$, $C$, $l$ are the molar absorption coefficient, molar concentration, and optical path length, respectively. Here, we approximate $\varepsilon$ of CBDAC at 440 nm in the UC film by that in methanol ($\varepsilon \cong 5.31 \times 10^4$ M$^{-1}$ cm$^{-1}$ @ 440 nm) based on the fact that the excitation spectrum of CBDAC in the UC film is similar to the absorption spectrum of CBDAC in methanol (*cf.* Fig. S10). From the mole ratio of CBDAC:PPO = 1:30,000 and the crystallographic density of PPO (*cf.* Section 6), $C$ of CBDAC in the PPO crystals was calculated to be ca. $1.92 \times 10^{-4}$ M.

The thickness of the sample film was 200 μm. However, considering that the optical path-length has been doubled by the aluminum reflection layer (*i.e.*, 2 × 200 μm = 400 μm), the absorbance was calculated to be ca. [$(5.31 \times 10^4$ M$^{-1}$ cm$^{-1}) \times (1.92 \times 10^{-4}$ M) × 0.04 cm] = 0.408, which corresponds to the *absorptance* of 60.9% at 440 nm. Using them, for $I_{th} \approx 14$ mW cm$^{-2}$ at 440 nm (Fig. 3b of the main text), the excitation rate ($k_{ex}$)[S6] and excitation density (ex)[S8] of CBDAC at $I_{th}$ are found to be ca. $7.7 \times 10^{-4}$ M s$^{-1}$ and ca. $2 \times 10^{16}$ s$^{-1}$ cm$^{-2}$, respectively. Note that the later value (ex) depends on the thickness of a film for the same $I_{th}$ because of its per-area definition.

## 12. Effect of annealing on $\Phi_{UC}$ and $I_{th}$

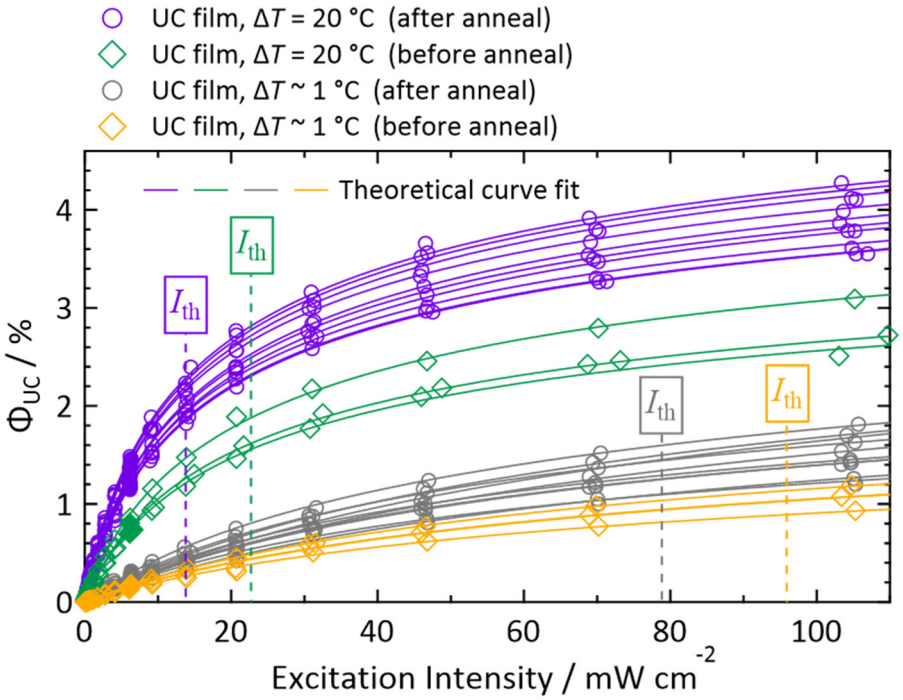


**Fig. S15**. Effect of annealing on the excitation intensity dependence of $\Phi_{UC}$. By annealing (see Section 1.4 for details), $\Phi_{UC}$ of "$\Delta T$ = 20 °C" and "$\Delta T$ ~ 1 °C" samples increased by ca. 38% and 35% on average, respectively; whereas $I_{th}$ of "$\Delta T$ = 20 °C" and "$\Delta T$ ~ 1 °C" samples decreased by ca. 34% and 15% on average, respectively.

## References


S1. V. Gray, K. Moth-Poulsen, B. Albinsson and M. Abrahamsson, *Coord. Chem. Rev.*, 2018, **362**, 54.

S2. Section 2.10 of J. R. Lakowicz, *Principles of Fluorescence Spectroscopy, 3rd Ed.*, Springer, New York, USA, 2006.

S3. J. N. Demas and G. A. Crosby, *J. Phys. Chem.*, 1971, **75**, 991.

S4. Y. Fujiwara, R. Ozawa, D. Onuma, K. Suzuki, K. Yoza and K. Kobayashi, *J. Org. Chem.*, 2013, **78**, 2206.

S5. R. Enomoto, M. Hoshi, H. Oyama, H. Agata, S. Kurokawa, H. Kuma, H. Uekusa and Y. Murakami, *Mater. Horiz.*, 2021, **8**, 3449.

S6. Y. Murakami and K. Kamada, *Phys. Chem. Chem. Phys.*, 2021, **23**, 18268.

S7. Y. Murakami, H. Kikuchi and A. Kawai, *J. Phys. Chem. B*, 2013, **117**, 5180.

S8. Y. Zhou, F. N. Castellano, T. W. Schmidt and K. Hanson, *ACS Energy Lett.*, 2020, **5**, 2322.